International Journal of Bifurcation and Chaos

A Heteroclinic Connection between two Saddle Slow Manifolds in the Olsen Model

Elle Musoke, Bernd Krauskopf and Hinke M. Osinga
Department of Mathematics, University of Auckland, Private Bag 92019
Auckland, 1142, New Zealand
elle.musoke@auckland.ac.nz

Received (to be inserted by publisher)

The abstract should summarize the context, content and conclusions of the paper. It should not contain any references or displayed equations. Typeset the abstract in 10 pt Times Roman with baselineskip of 12 pt, making an indentation of 1.6 cm on the left and right margins.

Keywords: A list of 3–5 keywords are to be supplied.

1. Introduction

Slow-fast dynamical systems are characterized by a separation of variables into those that evolve on a fast time scale and those that evolve on a slower time scale. The separation of variables into fast and slow can be found in many systems in the world around us: chemical systems, neurons, electric circuits, lasers, and predator-prey dynamics, among others, have been described by slow-fast models [Brøns & Bar-Eli, 1991; De Maesschalck & Wechselberger, 2015; Van der Pol, 1927; Otto *et al.*, 2012; Piltz *et al.*, 2017]. By reason of their ubiquity, the various phenomena that arise from the multiple-time-scale nature of slow-fast systems are of significant interest. These have been be described for two- and three-dimensional systems by well-established theory [Benoît *et al.*, 1981; Benoît, 1982, 1985; Guckenheimer, 1985; Brøns *et al.*, 2006; Krupa *et al.*, 2008]. In particular, small-amplitude limit cycles transitioning to larger-amplitude relaxation oscillations were studied in two dimensions, for example, the Van der Pol oscillator and FitzHugh–Nagumo model [Benoît *et al.*, 1981; FitzHugh, 1955]. In three-dimensional systems, periodic orbits with epochs of localized small-amplitude oscillations (SAOs) and epochs of large-amplitude oscillations (LAOs) have been observed [Hudson *et al.*, 1979]. The mechanisms that cause SAOs of these appropriately named mixed-mode oscillations (MMOs) are described in [Desroches *et al.*, 2012]. In this paper, we investigate novel phenomena that arise in four-dimensional slow-fast systems which may provide insight into undiscovered mechanisms for MMOs in higher-dimensional systems.

We consider a prototypical four-dimensional slow-fast dynamical system that exhibits MMOs, namely the so-called Olsen model for peroxidase-oxidase reaction that was first introduced by Lars F. Olsen in 1983 [Olsen, 1983]. The classification of variables as either slow or fast is not straightforward for the Olsen model because the variables are not consistently slow or fast over all regions of phase space. In fact, the Olsen model nominally has three different time scales. We focus specifically on a parameter regime corresponding to two different time scales with three fast and one slow variables. This parameter regime was also the focus in [Desroches *et al.*, 2009] which reports on a study of mechanisms for MMOs in the Olsen model were previously investigated in [Desroches *et al.*, 2009] after a model reduction. Manifolds on which the

Table 1. System parameters for system (1).

α	δ	ε	η	κ	μ	ζ
0.0912	1.2121×10^{-4}	0.0037	0.0540	3.7963	0.9697	0.9847

flow evolves on the slower time scale were computed along with the manifolds of trajectories converging to them in forward and backward time, respectively. These gave insight into the formation of MMOs, as well as the cause of their particular geometry. However, because of the assumptions used to reduce the model to a three-dimensional system, some of the computed manifolds were of lower dimension than the corresponding manifolds in the full system. In this research, we develop techniques for computing the same manifolds in the full four-dimensional model in the interest of studying their geometry and interactions with each other. In particular, we focus on interactions between higher-dimensional manifolds that do not exist in systems of three dimensions or lower.

The separation between fast and slow variables is more prominent if we use the change of coordinates described in [Kuehn & Szmolyan, 2015], which results in the following

$$\begin{cases} \frac{dA}{dt} &= \mu - \alpha A - ABY, \\ \frac{dB}{dt} &= \varepsilon(1 - BX - ABY), \\ \frac{dX}{dt} &= \frac{1}{\eta}(BX - X^2 + 3ABY - \zeta X + \delta), \\ \frac{dY}{dt} &= \frac{\kappa}{\eta}(X^2 - Y - ABY), \end{cases} \tag{1}$$

where $(A, B, X, Y) \in \mathbb{R}^4$ are positive concentrations of chemicals. The system parameters are the Greek letters and these have values as given in Table 1; they are functions of original system parameters given in [Olsen, 1983], and chosen to be the same as in [Kuehn & Szmolyan, 2015] with a minor modification (for notational convenience, we have substituted ε_b and ε^2 with ε and η, respectively).

The time-scaling parameters ε and η depend on the original system parameter k_1. As suggested by [Kuehn & Szmolyan, 2015], we decrease k_1 past 0.16 to 0.1 so that there are only two time scales. The parameters given in Table 1 correspond to a system with three fast variables, A, X and Y, and one slow variable, B.

This paper is organised as follows. In the next section we give the necessary background from geometric singular perturbation theory (GPST) for defining the manifolds which are the focus of this research. Section 3 gives definitions of the manifolds which are then computed in section 4. In section 5, a computation of an interaction between the manifolds computed in section 4 is described. Conclusions are given in section 6.

2. Background

The classical analysis of slow-fast systems considers the different so-called singular limits. In the limit as $\varepsilon \to 0$, the equation for B in system (1) reduces to $\frac{dB}{dt} = 0$ and system (1) can be viewed as the three-dimensional

$$\begin{cases} \frac{dA}{dt} &= \mu - \alpha A - ABY, \\ \frac{dX}{dt} &= \frac{1}{\eta}(BX - X^2 + 3ABY - \zeta X + \delta), \\ \frac{dY}{dt} &= \frac{\kappa}{\eta}(X^2 - Y - ABY), \end{cases} \tag{2}$$

for which B is a parameter. We refer to system (2) as the layer equation or the fast subsystem. If one first performs a time rescaling $\tau = \varepsilon t$, and then considers the limit as $\varepsilon \to 0$ the system reduces to

$$\begin{cases} 0 &= \mu - \alpha A - ABY, \\ \frac{dB}{d\tau} &= (1 - BX - ABY), \\ 0 &= \frac{1}{\eta}(BX - X^2 + 3ABY - \zeta X + \delta), \\ 0 &= \frac{\kappa}{\eta}(X^2 - Y - ABY), \end{cases} \tag{3}$$

which is a differential algebraic system called the slow subsystem or the reduced system. The three algebraic equations in system (3) define a one-dimensional manifold, called the critical manifold C. The flow in (3) is defined by the single differential equation for B and it is confined to C.

The critical manifold consists entirely of equilibria of the fast subsystem for different values of B. Their stability can be determined by the 3×3 Jacobian matrix of (2). Equilibria at which the Jacobian only has eigenvalues with non-zero real parts are called hyperbolic; otherwise we say that the equilibrium is non-hyperbolic. Non-hyperbolic equilibria correspond to local bifurcations of system (2). We consider a branch of the critical manifold to be a continuous curve of hyperbolic equilibria. In phase space, near a stable MMO of interest, the critical manifold has 11 branches separated from each other points at which there is a local bifurcation of the fast subsystem. We give the B values at which there is a bifurcation of the fast subsystem to three decimal places in the following paragraphs.

Figure 1 shows four branches of C projected into the (B,A)-plane. For these branches all variables are positive. Seven nearby branches of C are not shown, because they lie in regions where at least one of A, B, X, or Y is negative, so they are not physically relevant. Of the branches shown in Figure 1, the top most, black branch consists of stable equilibria of (2) and is separated from the teal-colored branch of saddle equilibria, denoted C^t, by a fold-point at, shown in orange and denoted F_1, occurring at $B = 0.956$. The fold F_1 has the appearance of a cusp in the (B,A)-projection, however (B, X)- and (B, Y)- projections show that this is truly a fold with respect to B. Another fold at $B = 0.273$, also shown in orange at and denoted F_2, separates C^t from a lower raspberry-colored branch of saddle equilibria. The raspberry branch of saddle equilibria is denoted C^b. It ends at $B = 0.897$ at a Hopf bifurcation, represented by the pink dot and denoted H. To the right of H, in black, is a stable branch of equilibria.

Equilibria $p \in C^t$ each have a two-dimensional stable eigenspace $E^s(p)$ and a one-dimensional linear unstable eigenspace $E^u(p)$. The flow of the full four-dimensional system (1) is from left to right near C^t in the (B, A)-projection shown. Equilibria on C^b have each one stable and two unstable eigenvectors. The flow is from right to left near C^b. We denote the local stable and unstable manifolds of points $p \in C$ by $W^s_{loc}(p)$ and $W^u_{loc}(p)$. These are the trajectories in (2) that converge to p in forward and backward time, respectively. By combining these manifolds for all $p \in C^t$, we find the saddle branch C^t has a three-dimensional local stable manifold $W^s_{loc}(C^t)$ and a two-dimensional local unstable manifold $W^u_{loc}(C^t)$ with respect to (2), which are defined as

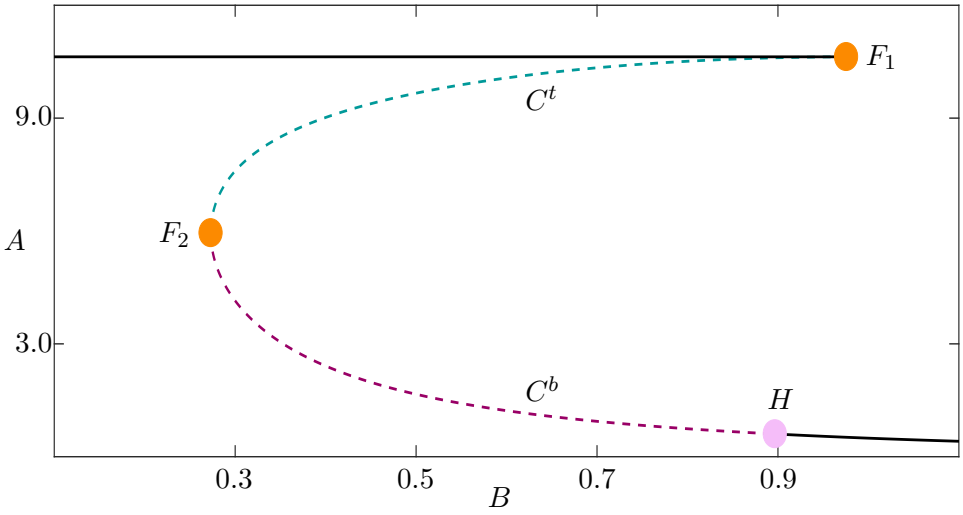

Fig. 1. Physically relevant branches of the critical manifold of system (1) shown in projection onto the (B,A)-plane. The branches labeled C^t and C^b and colored teal and raspberry, respectively, correspond to saddle equilibria of (2), solid curves indicate stable nodes. The two saddle-node bifurcations are represented as orange dots and labeled F_1 and F_2, respectively. The Hopf bifurcation is represented by a pink dot and is labeled H.

$$W^s_{loc}(C^t) = \bigcup_{p\in C^t} W^s_{loc}(p), \qquad W^u_{loc}(C^t) = \bigcup_{p\in C^t} W^u_{loc}(p).$$

Similarly C^b has a three-dimensional local unstable manifold $W^u_{loc}(C^b)$ and a two-dimensional local stable manifold $W^s_{loc}(C^b)$ with respect to system (2).

Although the branches C^t and C^b of the critical manifold are no longer invariant for $\varepsilon > 0$, Fenichel Theory guarantees that both C^t and C^b persist as locally invariant manifolds called slow manifolds, which we denote by S^t and S^b [Fenichel, 1979]. The slow manifold S^t has the same dimension as C^t and, as $\varepsilon \to 0$, it converges to C^t. Orbit segments that lie on a slow manifold remain slow for an $O(1)$ time with respect to the slow time scale. Locally invariant means that solutions can only enter or leave the manifold via its edges.

Due to its finite time nature, slow manifolds are not unique. We can select a unique representative S^t by considering the slow manifold that remains slow for the longest amount of time. Since equilibria of (2) lying on C^t are of saddle type, C^t and S^t are of saddle type. A unique slow manifold, S^b, associated with C^b can be defined similarly.

Fenichel Theory also guarantees that $W^s_{loc}(C^t)$ and $W^u_{loc}(C^t)$ persist as locally-invariant local stable and unstable manifolds of S^t [Fenichel, 1979]. We define the stable manifold of S^t as a family of orbit segments that have a fast approach to S^t and then stay close to it for $O(1)$ time with respect to the slow time scale. Similarly, we define the unstable manifold as a family of orbit segments, that approach S^t in backward time and then stay close to it for $O(1)$ (backward) time with respect to the slow time scale. According to Fenichel Theory, the stable and unstable manifolds of S^t have the same dimensions as $W^s_{loc}(C^t)$ and $W^u_{loc}(C^t)$ and lie at an $O(\varepsilon)$ distance away from them, respectively. We can similarly define the stable and unstable manifolds associated with C^b. To simplify notation later, we refer to these stable and unstable manifolds as W^s and W^u, respectively, and omit the specific reference to S^t and S^b. For both S^t and S^b, the manifolds W^s and W^u are not unique, but we can select a unique representative in a manner similar to that for S^t.

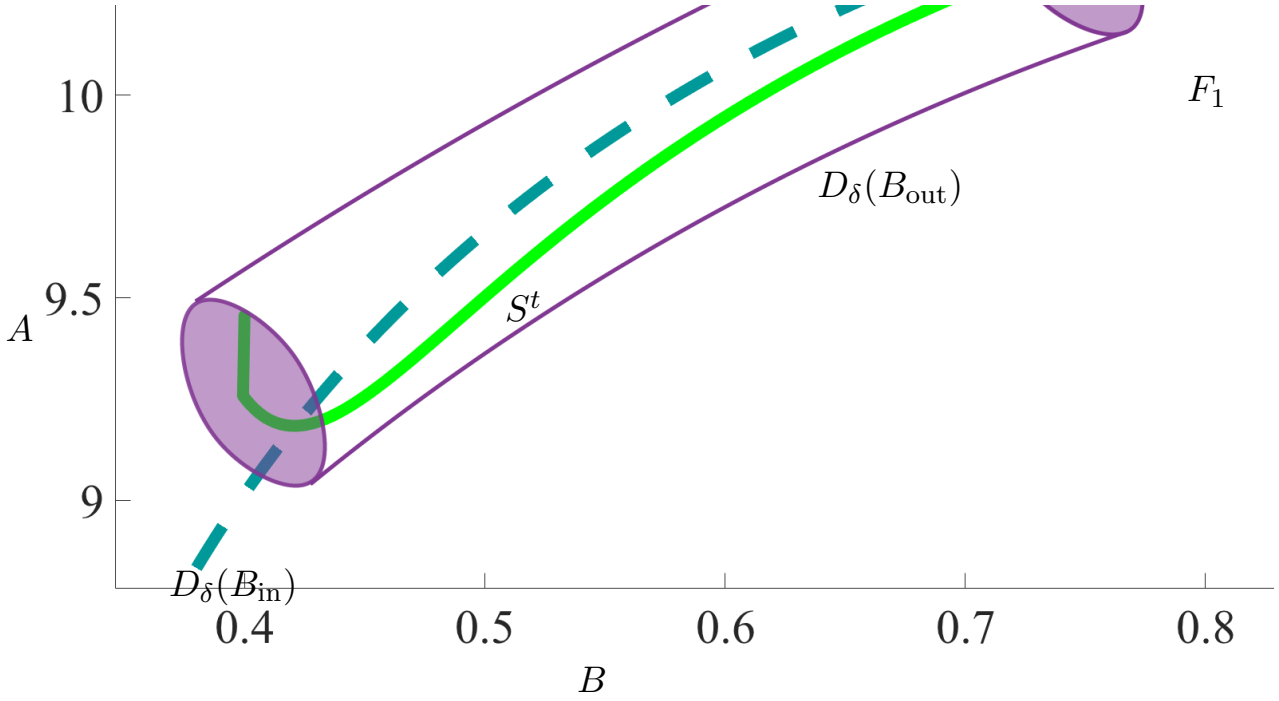

Fig. 2. The unique representative slow manifold S^t (green curve) projected into the (B, A)-plane. The spheres $D_\delta(B_{\text{in}})$ and $D_\delta(B_{\text{out}})$ are indicated by purple disks at either end of a four-dimensional cylinder, indicated by the purple curves.

3. Saddle Slow Manifolds and their (Un)Stable Manifolds

For the definition of a one-dimensional saddle slow manifold, we follow the presentation in [Farjami *et al.*, 2018] of an algorithm for the computation of a stable manifold of a one-dimensional saddle slow manifold for a three-dimensional system. Here we consider only the slow manifold S^t associated with C^t; the slow manifold S^b can be defined in a similar manner.

The precise definition of the slow manifold S^t is given with respect to a closed interval $[B_{\text{in}}, B_{\text{out}}]$ for the slow variable B. The values for B_{in} and B_{out} are chosen such that the interval is contained in the interval defined by the B-coordinates of the two fold points F_1 and F_2. Note that there is a segment in C^t for which each point $p \in C^t$ is uniquely associated via its B-coordinate with a value for $B_p \in [B_{\text{in}}, B_{\text{out}}]$. For each $B_p \in [B_{\text{in}}, B_{\text{out}}]$ there is a unique point $p = (p_A, p_B, p_X, p_Y) \in C^t$ such that $p_B = B_p$. We define a solid three-sphere $D_\delta(B_p)$ in the three-dimensional subsection $\{(A\ B\ X\ Y) \in \mathbb{R}^4 \mid B = p_B\}$ that has radius δ and center p, given formally by

$$D_\delta(B_p) = \{w \in \mathbb{R}^4 \mid w_B = B_p, \|w - p\| \leq \delta\}.$$

The union $\mathscr{D} = \cup_{B_p \in [B_{\text{in}}, B_{\text{out}}]} D_\delta(B_p)$ forms a four-dimensional compact cylinder. The radius δ is small, but it needs to be at least of $O(\varepsilon)$ to ensure that S^t lies in $\mathscr{D}$. The one-parameter family of orbit segments that enter $\mathscr{D}$ via $D_\delta(B_{\text{in}})$ and exit via $D_\delta(B_{\text{out}})$ are candidates for S^t. We impose the additional condition that S^t must have maximal integration time in $\mathscr{D}$ to select a unique representative. This condition may be interpreted as selecting S^t such that it enters $\mathscr{D}$ via W^s and exits via W^u.

This definition is similar to that given in [Farjami *et al.*, 2018], except that $D_\delta(B_{\text{in}})$ and $D_\delta(B_{\text{out}})$ are three-spheres rather than two-dimensional disks and $\mathscr{D}$ is four dimensional rather than three dimensional. Figure 2 shows the unique representative, S^t plotted in green, in projection onto the (B, A)-plane. Sketched in purple is $\mathscr{D}$ with the spheres $D_\delta(B_{\text{in}})$ and $D_\delta(B_{\text{out}})$ at either end; these spheres and $\mathscr{D}$ are for illustration.

Fenichel theory guarantees that each slow manifold S^t, associated with C^t, has a local, two-dimensional unstable manifold W^u_{loc} [Fenichel, 1979]. By definition, such an unstable manifold consists of a one-parameter family of orbit segments that have a fast approach to S^t in backward time before remaining

$O(\varepsilon)$ close for $O(1)$ (backward) slow time. Such an unstable manifold is not unique, but all manifolds in the family of a saddle slow manifold lie exponentially close to each other [Fenichel, 1979]. We select and approximate a specific candidate, W^u_{loc}, from this family of manifolds. Similarly there exists a local, non-unique, three-dimensional stable manifold $W^s_{\text{loc}}(S^t)$, which is defined as a two-parameter family of orbit segments that have a fast approach to S^t in forward time before remaining $O(\varepsilon)$ close for $O(1)$ slow time. Global unstable and stable manifolds W^u and W^s can be obtained from extending W^u_{loc} and W^s_{loc} in backward and forward time, respectively. In the lower-dimensional model considered in [Desroches *et al.*, 2009], the manifold W^s was two dimensional and computed in the region between C^t and C^b. We now turn to the computation of the three-dimensional manifold W^s of the full system in this same region.

4. Computations

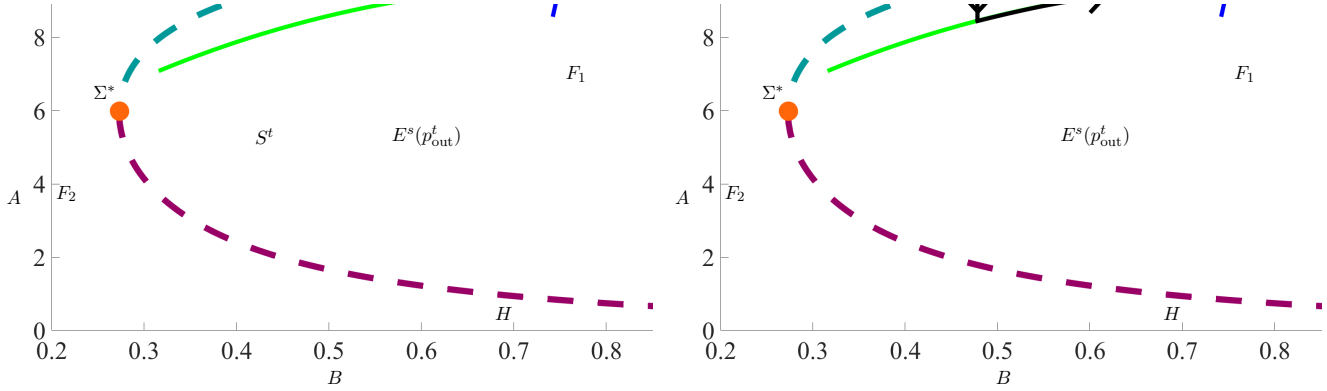

(a)A sketch of the first homotopy step in the algorithm for computing $W^s_{\Sigma^*}$. A projection of Σ^* is represented as a pink line in the (B, A)-plane. The linear stable space $E^s(p_{\text{out}})$ is represented by a blue cross while a sketch of S^t is shown in green.

(b)A representative orbit segment in the first homotopy step is represented as a black curve. Fast segments are represented with double arrows while slow segments are represented with single arrows.

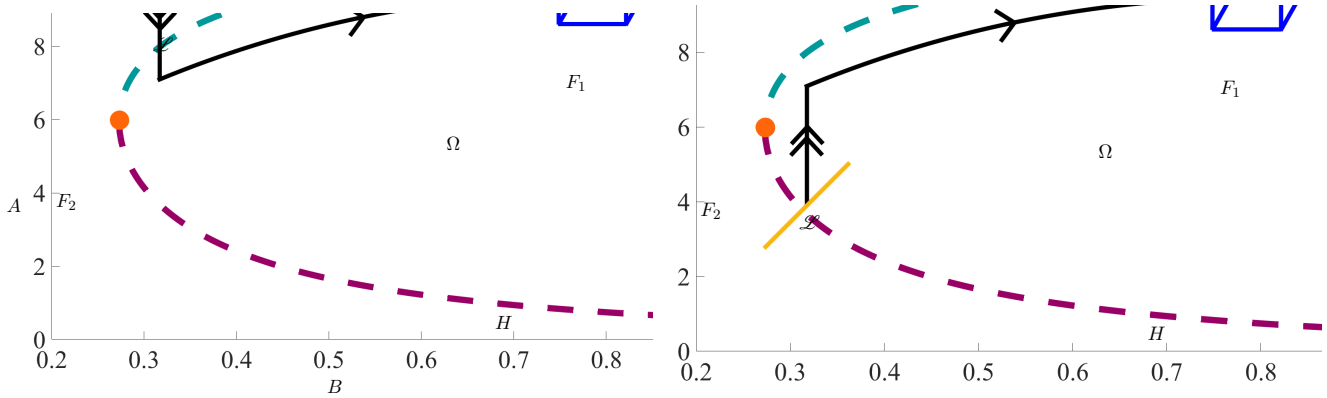

(c)A sketch illustrating the selection of an orbit segment with maximal integration time. Represented by a blue cube is the space Ω. The curve $\mathscr{L}$ is represented in yellow.

(d)A sketch of the selection of a different slice W^s_Σ. This representation shows a selection of Σ on the other side of the critical manifold from Σ^* in the (B, A)-projection.

Fig. 3. Set up for the computation of W^s_Σ.

As W^s is three dimensional it is challenging to compute and difficult to visualise. Research on computing and visualising three-dimensional manifolds is limited to a few examples from group theory and chemical sciences [Gunn, 1993; Wernli *et al.*, 2009]. At this time, there is no literature on the computation of three-dimensional stable manifolds of saddle slow manifolds in the slow-fast setting. Computing the entire three-dimensional manifold would require a two-dimensional mesh of collocation points which is computa-

tionally expensive compared to the on-dimensional mesh of collocation points needed for the computation of two-dimensional manifolds. A natural way forward is to consider a subset of W^s as a one-parameter family of two-dimensional slices. These can be visualised and computed with the pseudo-arclength continuation package AUTO [Doedel, 2007]. We begin by defining a two-dimensional plane Σ given by fixed values of A and either X or Y. We approximate a slice with a smooth, one-parameter family of solutions to 4 $\mathbf{u}$ that begin in Σ, enter $\mathscr{D}$ at $D_\delta(B_p)$ for some $B_p \in [B_{\text{in}}, B_{\text{out}}]$, and remain inside $\mathscr{D}$ for $O(1)$ slow time. We use W^s_Σ to denote such an approximation. The slice W^s_Σ is taken to be the collection of those parts of $\mathbf{u}$ that enter $\mathscr{D}$ in the fast direction. The later parts that evolve mostly in the B-direction inside $\mathscr{D}$ for $O(1)$ slow time are considered to represent approximate parts of S^t. If the later part of the orbit segment $\mathbf{u}$ includes a fast exit from $\mathscr{D}$, that fast part is considered as an approximation of an orbit segment lying on W^u.

We first explain the computation of W^s_Σ for the specific plane $\Sigma = \Sigma^*$, given by fixing A- and Y-coordinates of the point $p_{\text{out}} \in C^t$ such that $p_B = B_{\text{out}} = 0.9$, where we adapted the technique outlined in [Farjami *et al.*, 2018] for two-dimensional stable manifolds in three-dimensional systems. We then explain the computation of W^s_Σ for an arbitrary plane Σ that is transverse to the flow as well as $\bigcup_{p\in C^t} E^u(p)$ in our region of interest.

The computation of slices of the three-dimensional unstable manifold W^u associated with S^b is more complex than that of S^t. The two extra challenges are a saddle equilibrium of the full system lying on C^b at $B = 0.323$ and the Hopf bifurcation of the fast subsystem at $B = 0.897$. Additional care must be taken to ensure that the computed orbits do not increase in integration time by approaching the saddle equilibrium's stable manifold or by following the nearby stable slow manifold backward in time. We modify the steps for computing two-dimensional slices of W^s associated with S^t in order to ensure that an increase in integration time results only from a more accurate approximation of a slice of W^u associated with S^b.

4.1. *The stable manifold associated with S^t*

We view S^t as an orbit segment $\mathbf{u} = \{\mathbf{u}(s) | 0 \le s \le 1\}$ of the rescaled system

$$\frac{d\mathbf{u}}{ds} = TF(\mathbf{u}), \tag{4}$$

where $\mathbf{u}(s) = (A(s), B(s), X(s), Y(s)) \in \mathbb{R}^4$ is the vector of chemical concentrations, F is the right-hand side of (1) and T is the total integration time on the fast timescale, $t = Ts$.

As in section 3.1, we obtain a first solution on $W^s_{\Sigma^*}$ via a homotopy step. Following the definition for $W^s_{\Sigma^*}(S^t)$, we set

$$\mathbf{u}(0) \in \Sigma^* \tag{5}$$

that imposes two conditions on $\mathbf{u}(0)$, since Σ^* is two dimensional. As part of selecting a solution $\mathbf{u}$ that has a fast approach and remains close to S^t for $O(1)$ slow time, we consider the two-dimensional eigenspace $E^s(p^t_{\text{out}})$ that is transverse to W^u. We define the boundary condition

$$\mathbf{u}(1) \in E^s(p^t_{\text{out}}) \tag{6}$$

that imposes two conditions on $\mathbf{u}(1)$ and allows for the possibility of $\mathbf{u}(1)$ intersecting W^u. The point p_{out} is a solution to the 2PBVP defined by (4), (5) and (6) with $T = 0$. Figure 3(a) illustrates an example of the set up for this homotopy step in projection onto the (B, A)-plane. Here, the plane Σ^* is projected to a line (pink), $E^s(p^t_{\text{out}})$ is represented by a blue cross, and a curve representing S^t is sketched in neon green.

We increase the total integration while allowing the B-coordinate value of $\mathbf{u}(0)$ to decrease towards F_2. Note that increasing integration time in this fashion corresponds to negative T. This step is illustrated in Figure 3(b) where an intermediate orbit is represented as a black curve clearly illustrating the presence of a fast segment (double arrows) followed by a slow segment (single arrow). The continuation is stopped just

before $\mathbf{u}(0)_B$ reaches the B-coordinate value of F_2, at $\mathbf{u}(0)_B = B_{\text{in}} = 2.3 \times 10^{-1}$. A sketch of the resulting orbit segment is shown in Figure 3(c).

The orbit segment illustrated in Figure 3(c) belongs to a two-parameter family of solutions $\mathbf{u}$ of (4) that satisfy the boundary conditions (5) and (6). To select a one-parameter family of orbit segments from these, we select for each $B \in [B_{\text{in}}, B_{\text{out}}]$ the solution $\mathbf{u}(t)$ to (4) with maximal integration time such that $\mathbf{u}(0)_B$. To find an initial orbit segment satisfying this condition, we define the curve $\mathscr{L} = \Sigma^* \cap \{(A\ B\ X\ Y) \in \mathbb{R}^4 | B = B_{\text{in}}\}$ and require

$$\mathbf{u}(0) \in \mathscr{L}, \tag{7}$$

which imposes three conditions on $\mathbf{u}(0)$ and is more restrictive than (5). The boundary condition (7) is represented as a yellow line in Figure 3(c). We can then lessen the restrictions on $\mathbf{u}(1)$ and define the three-dimensional space Ω spanned by the two stable eigenvectors of p_{out} and the vector parallel to the B-direction. Note that Ω is transverse to $\cup_{p \in C^t} E^u(p)$ and hence W^u. Instead of (**??**BC7)) we require

$$\mathbf{u}(1) \in \Omega, \tag{8}$$

which imposes only one condition on $\mathbf{u}(0)$. Condition (8) is represented in Figure 3(c) as a cube with dark blue edges. We now track the solution $\mathbf{u}(t)$ of the 2PBVP (4),(7),(8) as T decreases; this causes $\mathbf{u}(0)$ to approach $W^s \cap \Sigma^*$ and $\mathbf{u}(1)$ to approach $W^u \cap \Omega$. When a fold in T is reached $\mathbf{u}(0)$ and $\mathbf{u}(1)$ have intersected W^s and W^u, respectively, and a (local) minimum in T time is attained.

The orbit segment that is obtained is not shown as it is almost identical to the orbit segment illustrated in Figure 3(c). It begins in Σ^* and has a fast approach to S^t before remaining $O(\varepsilon)$ close for $O(1)$ slow time, and so it lies on $W^s_{\Sigma^*}$ by definition. In addition to finding an orbit that approximates a solution to (4) laying on S^t, we can approximate S^t itself by restricting the orbit segment further inside $[B_{\text{in}}, B_{\text{out}}]$ to exclude fast segments. We are now ready to compute the entire solution family on $S^s_{\Sigma^*}$ by continuation of the fold in T, while allowing $u(0)_B$ to increase.

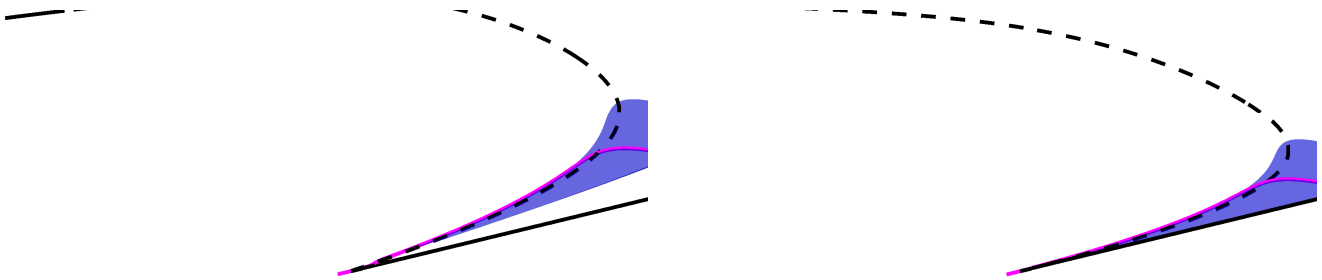

(a) (b)

Fig. 4. The slice $W^s_{\Sigma^*}$, represented in blue, projected into (B, A, X)-space (a) and (B, A, Y)-space (b) with a representative orbit segment plotted in magenta. Projections of the critical manifold are shown in black and the view is rotated relative to previous figures.

Figure 4 shows two projections of $W^s_{\Sigma^*}$. Although the manifold is two dimensional, it is necessary to visualise it in both (B, A, X)- and (B, A, Y)-projections because it exists in four-dimensional space. Lying on $W^s_{\Sigma^*}$ is a representative orbit segment, plotted in magenta. The critical manifold is plotted in black. The view is rotated relative to earlier figures to help illustrate the geometry of the slice. Orbits lying on $W^s_{\Sigma^*}$ have a fast approach to S^t in X and Y before approaching mainly in the A-direction and then finally remaining close to C^t for $O(1)$ slow time.

In the case where we would like to compute W^s_{Σ} for a different Σ, given by constant values of A and Y (respectively X), we must perform a second homotopy step after the first. Using the orbit segment

represented in Figure 3(c) as a starting point, we impose (6) while keeping as free parameters T, $\mathbf{u}(0)_B$, and the X-coordinate value of $\mathbf{u}(0)$, $\mathbf{u}(0)_X$ (respectively the Y-coordinate value of $\mathbf{u}(0)$, $\mathbf{u}(0_Y)$). In two runs, we continue $\mathbf{u}$ with $\mathbf{u}_A(0)$ and $\mathbf{u}(0)_Y$ (respectively $\mathbf{u}(0)_X$) as main continuation parameters. In each of these runs, we increase or decrease the main continuation parameter until it attains the value necessary for $\mathbf{u}(0) \in \Sigma$. Once $\mathbf{u}(0) \in \Sigma$, we follow the rest of the procedure above while considering Σ instead of Σ^*.

Figure 3(d) illustrates a choice of Σ on the opposite side of the critical manifold from Σ^* in the (B, A)-projection. The orbit segment resulting from the second homotopy step is represented as a black curve. Conditions (7) and (8) are again illustrated with a yellow line and a cube with dark blue edges, respectively.

Figure 6 shows $W^s_{\Sigma^*}$ together with four other slices W^s_Σ of W^s. The additional slices were selected with Σ given by $A = 2.0$ and $Y = 2.3001 \times 10^{-4}$, $A = 4.0$ and $X = 0.75$, $A = 4.0$ and $Y = 0.75$, and $A = 6.0$ and $X = 0.5$, accurate to four decimal places. The slices appear to have (self)intersections in each projection, but they do not intersect themselves or eachother in the full four-dimensional space.

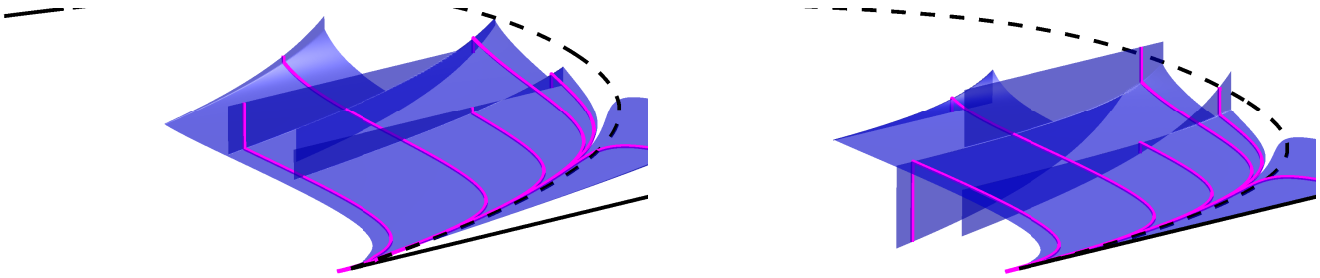

(a) (b)

Fig. 5. A variety of submanifolds W^s_Σ (blue) of the stable manifold W^s of the saddle slow manifold S^t projected into (B, A, X)-space (a) and (B, A, Y)-space (b) with example orbit segments plotted in magenta. Projections of the critical manifold are shown in black and the view is rotated relative to previous figures.

We note that, unlike the stable manifold of S^t computed for the reduced system in [Desroches *et al.*, 2009], each slice W^s_Σ in Figure 6 diverges backwards in time in the X- and Y- directions before reaching S^b. The computations in [Desroches *et al.*, 2009] suggest that there exists a submanifold of W^s in the four-dimensional system that spirals around S^b in backward time for an appropriate choice of Σ. Such a surface would be the intersection of the two three-dimensional manifolds W^s and W^u in the full four-dimensional system. A heteroclinic connection between two saddle slow manifolds is not a phenomenon that can occur in three-dimensional systems.

4.2. *The unstable manifold associated with S^b*

We begin by defining for each $B_p \in [B_{\text{in}}, B_{\text{out}}]$ a two-dimensional sphere

$$\bar{D}_r(B_p) = \{w \in \mathbb{R}^4 | w_B = B_p, |w - p| = r\}$$

where $p \in C^b$ is the unique point such that $p_B = B_p$. We can then define the three-dimensional cylinder $\mathscr{R} = \cup_{B \in [B_{\text{in}}, B_{\text{out}}]} \bar{D}_r(B)$. A slice W^u_r is defined as a smooth, one parameter family of orbit segments $\mathbf{u}$ that enter $\mathscr{D}$ at $D_\delta(B_{in})$ and exit at $B_p \in (B_{\text{in}}, B_{\text{out}})$ before intersecting $\mathscr{R}$. In the following steps, the computation of a slice $W^u_{r^*}$ is outlined for $r^* = 0.7$ before the description of the necessary modifications to obtain W^u_r for more general r.

We perform an initial homotopy step to obtain an orbit segment that enters $\mathscr{D}$ at B_{in} and intersects $\mathscr{R}$ after exiting $\mathscr{D}$ at some $B^* \in (B_{\text{in}}, B_{\text{out}})$. We select the unique point $p^* \in C^b$ such that $p^*_B = 0.7$. The plane $\bar{\Sigma}$ is defined by fixing the A- and Y- coordinates of p^*. We impose the boundary conditions

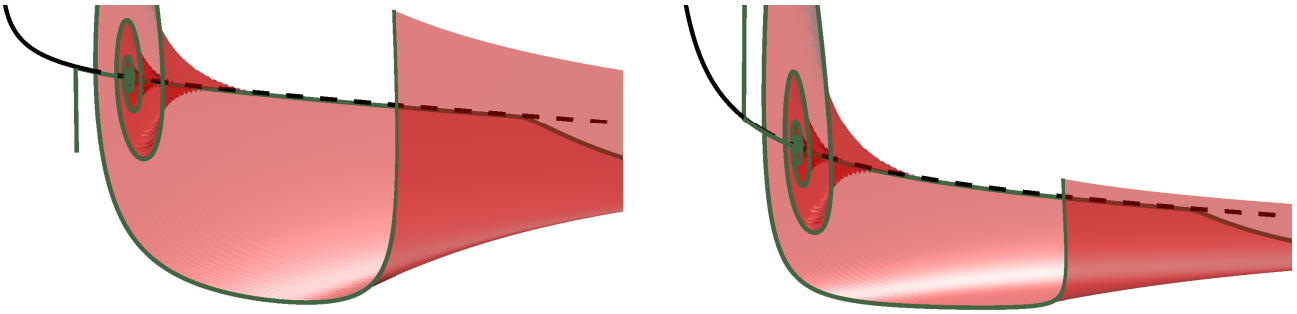

(a) (b)

Fig. 6. The slice $W^u_{r^*}$ of W^u is represented in red, projected into (B, A, X)-space (a) and (B, A, Y)-space (b) with example orbit segments plotted in forest green. Projections of the critical manifold are shown in black and the view is rotated relative to previous figures.

$$\mathbf{u}(0) \in E^u(p^*), \tag{9}$$

and

$$\mathbf{u}(1) \in \bar{\Sigma} \tag{10}$$

which each impose two conditions on $\mathbf{u}(0)$ and $\mathbf{u}(1)$ respectively. The point p^* is then a solution to the 2PBVP defined by (4), (9), and (10) for $T = 0$. We increase T while $\mathbf{u}(0)_B$ decreases and stop the continuation when $\mathbf{u}(1)$ intersects $\mathscr{R}$. We denote by B_{stop} the B-value of $\mathbf{u}(1)$ at the end of this step.

In the second homotopy step we define a three-dimensional space $\phi_{\text{HOM2}} = \{E^u(p^*) + \begin{bmatrix}0 & B & 0 & 0\end{bmatrix}^T | B \in \mathbb{R}\}$ and a one-dimensional circle $\mathscr{L} = \{w \in \mathbb{R}^4 | w_Y = p^*_Y, w_B = B_{\text{stop}}, |w - p^{\text{stop}}| = 0.7\}$ where $p^{\text{stop}} \in C^b$ is the unique point such that $p^{\text{stop}} = B_{\text{stop}}$. We then impose the boundary conditions

$$\mathbf{u}(0) \in \phi_{\text{HOM2}}, \tag{11}$$

and

$$\mathbf{u}(1) \in \mathscr{L}. \tag{12}$$

Condition (11) imposes one condition on $\mathbf{u}(0)$ while condition (12) imposes three conditions on $\mathbf{u}(1)$. The orbit segment resulting from the first homotopy step is a solution to the 2PBVP defined by (4), (11), and (12). We continue the orbit segment by increasing T while $\mathbf{u}(0)_B$ increases. The continuation is stopped when $\mathbf{u}(0)_B = B_{\text{in}} = 1.0$.

We define the plane $\Phi = \{w \in \phi_{\text{HOM2}} | w_B = B_{\text{in}}\}$ and impose the boundary conditions

$$\mathbf{u}(0) \in \Phi, \tag{13}$$

and

$$\mathbf{u}(1) \in \mathscr{R} \cap \{w \in \mathbb{R}^4 | w_B = B_{\text{stop}}\} \tag{14}$$

which impose two conditions on $\mathbf{u}(0)$ and $\mathbf{u}(1)$ respectively. The orbit segment resulting from the second homotopy step is a solution to the 2PBVP defined by (4), (13), and (14). Our aim is to select a smooth one-parameter family of orbit segments from the two-parameter family of orbit segments satisfying (13)

and (14). To this end, for each $B_p \in [B_{\text{in}}, B_{\text{out}}]$, we select from the one-parameter family of orbit segments exiting $\mathscr{D}$ at B_p the orbit segment with maximal integration time. To find an initial orbit of this description we increase T again until maximal integration time is reached. This is detected as a fold in T. Finally to obtain the rest of the slice $W^u_{r^*}$ we switch the endpoint boundary condition to

$$\mathbf{u}(1) \in \mathscr{R} \tag{15}$$

which imposes one condition on $\mathbf{u}(1)$. In two runs, the fold in T is continued until $\mathbf{u}(0)_B = B_{\text{out}}$ and then again until $\mathbf{u}(0)_B = B_{\text{in}}$ to sweep out $W^u_{r^*}$.

We can compute a different slice W^u_r by returning to the second homotopy step in our computation. Depending on the magnitude of r, we may need to perform one or two additional homotopy steps. In the case where r is large enough that $D^*_r(\mathbf{u}(1)_B)$ contains a locus of points at which the flow is tangent to it, an extra homotopy step is needed. We define a plane ϕ_{hom3} by fixing the A- and X-coordinates of $\mathbf{u}(1)$ after the second homotopy step. The orbit is continued with the boundary conditions (13) and

$$\mathbf{u}(1) \in \phi_{\text{hom3}}, \tag{16}$$

which imposes two conditions on $\mathbf{u}(1)$. The endpoint B-coordinate $\mathbf{u}(1)_B$ is increased until $D^*_r(\mathbf{u}(1)_B)$ no longer contains a locus of tangent points.

The final homotopy step involves defining another plane ϕ_{homfinal} by fixing the B- and X- values of $\mathbf{u}(1)$. Condition (13) is imposed while a new restriction

$$\mathbf{u}(1) \in \phi_{\text{homfinal}}, \tag{17}$$

imposes two conditions on $\mathbf{u}(1)$. The radius r is then increased or decreased until the desired magnitude is attained. All that remains is to follow through with the rest of the steps to compute W^u_r.

References

Benoît, E. [1982] "Systèmes lents-rapides dans $\mathbb{R}^3$ et leurs canards," *Proceedings of the Third Schnepfenried Geometry Conference* **2**, 159–191.

Benoît, E. [1985] "Enlacements de canards," *Comptes Rendus Mathematique Academie des Sciences* **300**, 225–230.

Benoît, E., Callot, J. F., Diener, F. & Diener, M. [1981] "Chasse au canard," *Collectanea Mathematica* **31**, 37–119.

Brøns, M. & Bar-Eli, K. [1991] "Canard explosion and excitation in a model of the belousov-zhabotinskii reaction," *Journal of Physical Chemistry A* **95**, 8706–8713.

Brøns, M., Krupa, M. & Wechselberger, M. [2006] "Mixed mode oscillations due to the generalized canard phenomenon," *Fields Institute Communications* , 39–63.

De Maesschalck, P. & Wechselberger, M. [2015] "Neural Excitability and Singular Bifurcations." *The Journal of Mathematical Neuroscience* **5**.

Desroches, M., Guckenheimer, J., Krauskopf, B., Kuehn, C., Osinga, H. & Wechselberger, M. [2012] "Mixed-Mode Oscillations with Multiple Time Scales." *SIAM Review* **54**, 211–288.

Desroches, M., Krauskopf, B. & Osinga, H. [2009] "The geometry of mixed-mode oscillations in the Olsen model for peroxidase-oxidase reaction." *Discrete & Continuous Dynamical Systems* **2**, 807–827.

Doedel, E. [2007] *AUTO-07p: Continuation and Bifurcation Software for Ordinary Differential Equations*, URL http://indy.cs.concordia.ca/auto/, with major contributions from A.R. Champneys, F. Dercole, T.F. Fairgrieve, Y.A. Kuznetsov, R.C. Paffenroth, B. Sandstede, X. Wang and C. Zhang.

Farjami, S., Kirk, V. & Osinga, H. [2018] "Computing the Stable Manifold of a Saddle Slow Manifold." *SIAM Journal on Applied Dynamical Systems* **17**, 350–379.

Fenichel, N. [1979] "Geometric singular perturbation theory for ordinary differential equations," *Journal of Differential Equations* **31**, 53–98.

FitzHugh, R. [1955] "Mathematical models of threshold phenomena in the nerve membrane," *The bulletin of mathematical biophysics* **17**, 257–278.

Guckenheimer, J. [1985] "Singular hopf bifurcation in systems with two slow variables," *SIAM Journal on Applied Dynamical Systems* **7**, 1355–1377.

Gunn, C. [1993] "Discrete groups and visualization of three-dimensional manifolds, (anaheim, california, august 1-6, 1993," *Proceedings of SIG–GRAPH '93*, ed. SIGGRAPH, A., Computer Graphics Proceedings, Annual Conference Series, 1993 (The publisher, New York), pp. 255–262, an optional note.

Hudson, J. L., Hart, M. & Marinko, D. [1979] "An experimental study of multiple peak periodic and nonperiodic oscillations in the belousov–zhabotinskii reaction," *The Journal of Chemical Physics* **71**, 1601–1606.

Krupa, M., Popović, N. & Kopell, N. [2008] "Mixed-mode oscillations in three time-scale systems: A prototypical example," *SIAM Journal on Applied Dynamical Systems* , 361–420.

Kuehn, C. & Szmolyan, P. [2015] "Multiscale Geometry of the Olsen Model and Non-classical Relaxation Oscillations." *Journal of Nonlinear Science* **25**, 583–629.

Olsen, L. [1983] "An enzyme reaction with a strange attractor." *Physics Letters A* **94**, 454–457.

Otto, C., Ludge, K., Vladimirov, A. G., Wolfrum, M. & Scholl, E. [2012] "Delay-induced dynamics and jitter reduction of passively mode-locked semiconductor lasers subject to optical feedback," *New Journal of Physics* **14**.

Piltz, S. H., Veerman, F., Maini, P. K. & Porter, M. A. [2017] "A predator–2 prey fast–slow dynamical system for rapid predator evolution," *SIAM Journal on Applied Dynamical Systems* **16**, 54–90.

Van der Pol, B. [1927] "Forced oscillations in a circuit with non-linear resistance. (Reception with reactive triode)." *The London, Edinburgh, and Dublin Philosophical Magazine and Journal of Science* **3**, 65–80.

Wernli, M., Caruso, D., E., B. & Gianturco, F. A. [2009] "Computing a three-dimensional electronic energy manifold for the $\mathrm{LiH} + \mathrm{H} \rightleftharpoons \mathrm{Li} + \mathrm{H_2}$ chemical reaction," *Journal of Physical Chemistry A* **113**, 1121–1128.